AIMS Mathematics, 11(3): 7078–7097.
DOI:10.3934/math.2026291
Received: 23 January 2026
Revised: 27 February 2026
Accepted: 09 March 2026
Published: 18 March 2026

https://www.aimspress.com/journal/Math

Research article

Numerical approach for solving the inverse problem: A two-dimensional time-fractional boundary value problem

Mousa J. Huntul[1,*] **and Mahmut Modanli**[2,*]

[1] Department of Mathematics, College of Science, Jazan University, P. O. Box 114, Jazan 45142, Saudi Arabia

[2] Department of Mathematics, Faculty of Arts and Sciences, Harran University, Şanlıurfa 63300, Türkiye

* **Correspondence:** Email: mhantool@jazanu.edu.sa, mmodanli@harran.edu.tr.

Abstract: This paper presents the inverse problem (IP) for the fractional order two-dimensional parabolic diffusion equation (FOTDPDE) formulated to depend on a initial-boundary value problem (IBVP) with homogeneous Dirichlet boundary conditions (DBC). The model involves a fractional-order Caputo derivative (FOCD) and an inverse time-dependent source term. A Crank-Nicholson finite difference scheme (CN-FDS) is constructed, and stability inequalities and a theorem in the discrete L^2 norm are proved to ensure unconditional stability of the proposed scheme. Results calculated by using finite difference methods (FDM) have a temporal convergence rate of $O(\tau^{2-\alpha})$ and second-order spatial accuracy. Numerical examples are tested to confirm the theoretical stability results and to represent the effectiveness and the accuracy of the method for solving IP for FOTDPDE depending on BVP.

Keywords: inverse problem for two-dimensional time Caputo fractional order equation; Crank–Nicolson finite difference scheme; initial and boundary value problem; finite difference method; stability estimates
Mathematics Subject Classification: 35K15, 65N06, 65N12

1. Introduction

Partial differential equations (PDEs) depending on IBVP appear naturally in the mathematical modeling of space sciences, physical, biological, and engineering systems, as well as artificial intelligence. Classical PDEs have been widely applied to describe transport phenomena; nevertheless, these equations often don't have hereditary effects or efficient memory observed in complex media. Fractional-order partial differential equations (FOPDEs), which associate derivatives of non-integer order, give a powerful tool generalization capable of modeling anomalous diffusion equations and

very long-range temporal dependence. Among fractional models, the time-dependent fractional inverse problem for FOTDPDE with Caputo derivatives has gained significant interest due to its ability to associate physically meaningful initial conditions. However, the non-local nature of the FOCD significantly complicates both theoretical analysis and numerical calculations, particularly in multidimensional boundary value problems.

In the study [1], the IP of the pseudo-parabolic equation (PPE) depended on a p-Laplacian operator, and a non-local integral condition was investigated. They addressed an inverse source problem for a nonlinear p-Laplacian PDE involving a time FOCD [2]. A time-fractional diffusion differential equation, together with suitable initial and boundary value conditions, was studied in both n-dimensional whole-space and half-space domains [3]. A time-fractional order parabolic equation with a parallel CN-FDM for on a distributed system was investigated [4]. They investigated third-order PDE with FOCD and Atangana–Baleanu (AB) derivative [5]. They applied two numerical methods for the mobile-immobile advection-dispersion model [6]. However, many papers have studied IP in the literature [7–9]. They investigated a two-dimensional (2D) time-fractional order inverse diffusion problem by using a modified kernel method [10].

Recent studies have proved that inverse problems for fractional order diffusion equations were typically ill-posed and required stable numerical schemes and regularization techniques [11, 12]. In order to handle the inverse Cauchy problem related to the fractional heat conduction equation in functionally graded materials (FGMs), a generalized finite difference method (GFDM) based on a localized meshless collocation framework was adopted [13]. The article employs the singular boundary method (SBM), a semi-analytical boundary fitting strategy, together with the double reciprocity method (DRM) and Laplace transform, to solve anomalous heat conduction problems occurring in functionally graded materials (FGMs) [14]. In recent years, the time-fractional diffusion-wave equation (TFDWE) has been studied using the iterative weighted Tikhonov regularization technique (IWTRT) [15]. In [16], an algorithm was developed to address the inverse as well as the direct problem for a fractional-order differential equation model, where derivatives with respect to space and time are of non-integer order. Using the Riemann–Liouville fractional derivative, an approximate symmetry method was developed for n-dimensional time-fractional PDEs with a small perturbation parameter [17].

The development of accurate numerical methods stable for fractional order boundary value problems stays an active area of research. Finite difference methods (FDMs) are especially attractive by virtue of their simplicity and ease of application.

In this work, we attempt to construct an efficient CN-FDS for the inverse problem of the two-dimensional time-fractional diffusion equation subject to homogeneous DBCs. The main contributions of this paper are the explicit formulation of BVP, the construction of a fully discrete FDS, and the rigorous proof of unconditional stability estimates.

In this paper, we shall investigate the following IP for the two-dimensional time-fractional order diffusion equation (TDTFODE) governed by the FOCD:

$$ {}_0^C D_t^\alpha w(x,y,t) = \Delta w(x,y,t) + v(t)S(x,y) + f(x,y,t), \quad (x,y) \in \Omega,\ 0 < t \le T, \tag{1.1} $$

where $0 < \alpha \le 1$, $v(t) = t^2$ is a known temporal modulation function, and $S(x,y)$ is an *unknown spatial source term* to be identified. Let $\Omega = (0,l) \times (0,l)$ be a bounded space domain, and let $0 < T < \infty$ demonstrate the final time. Let $w(x,y,t)$ satisfy a TDTFODE with unknown parameter $S(x,y)$. The

inverse problem is to reconstruct $S(x, y)$ from given additional data:

$$w(x, y, t)|_{\Gamma\times(0,T]} = g(x, y, t),$$

where Γ denotes a measurement boundary or interior observation domain. We investigate an IP for a TDTFODE. The IP consists of determining an unknown parameter (or source term/coefficient) in the governing equation from additional measurement data, such as boundary or interior observations of the solution. The Laplace operator $\Delta w(x, y, t)$ in two spatial dimensions is presented by

$$\Delta w(x, y, t) = w_{xx}(x, y, t) + w_{yy}(x, y, t). \tag{1.2}$$

The model is presented with the initial condition

$$w(x, y, 0) = w_0(x, y), \quad (x, y) \in \Omega, \tag{1.3}$$

and given by homogeneous DBC

$$w(x, y, t) = 0, \quad (x, y) \in \partial\Omega,\ 0 \le t \le T. \tag{1.4}$$

For the purpose of uniquely stating the unknown source term $S(x, y)$, an additional measurement is stated in the form of a last-time observation:

$$W_T(x, y) = w(x, y, T), \quad (x, y) \in \Omega, \tag{1.5}$$

where $W_T(x, y)$ demonstrates the observed data at the terminal time. FOCD is defined as in [18] for $0 < \alpha \le 1$:

$$ {}_0^C D_t^\alpha w(t) = \frac{1}{\Gamma(1-\alpha)} \int_0^t (t-s)^{-\alpha} \frac{\partial w(s)}{\partial s}\, ds.$$

Now, we can defined the inverse problem statement as the following: Given the initial data $w_0(x, y)$, the boundary condition (1.4), the last-time measurement $W_T(x, y)$, and the function $v(t)$, the inverse problem involves determining the unknown pair $\{w(x, y, t),\ S(x, y)\}$ such that eqs (1.4) and (1.5) are satisfied. It is well known that the inverse source problems for TDTFODE are typically defined as ill-posed in the Hadamard sense, meaning that the solution may not exist, may not be unique, or may not be continuously dependent on the data. For the TDTFODE (1.1), the uniqueness of the spatial source term $S(x, y)$ can be ensured under appropriate final or internal observation data and appropriate regularity assumptions. Furthermore, stability estimates can be obtained using energy methods or fractional Grönwall-type inequalities, and it can be shown that small distortions in the measurement data lead to limited distortions in the reconstructed source term. These properties justify the development of robust numerical schemes to solve the IP.

The importance of the model (1.1) can be given as follows. The inverse problem of (1.4) and (1.5) naturally arises in a great deal of applied fields where the intrinsic source of a diffusion process cannot be directly measured. In groundwater and environmental engineering, the unknown source term represents pollutant release sites in porous media. In thermal engineering, the inverse problem corresponds to intrinsic heat generation in materials with memory effects. In biomedical implementations, the model presents anomalous transport processes in heterogeneous biological tissues. The use of time FOCD allows the model to capture memory and inherited effects that

cannot be represented by classical diffusion equations. However, the presence of non-local temporal dynamics makes the inverse problem ill-defined; that is, small distortions in the observational data can evoke large reconstruction errors. This situation makes the development and practicality of stable numerical methods essential. Inverse source identification for the two-dimensional formulation with homogeneous boundary conditions satisfies a mathematically realistic and physically meaningful framework. Finally, this model yields as an important benchmark problem for the analysis and approximate solution of inverse fractional order boundary value problems.

The main contributions of this paper are: (i) development of a CN-FDS method for the inverse problem in TDTFODE with IBVP; (ii) theoretical analysis of convergence and stability of the proposed numerical CN-FDS; (iii) extensive exact and approximate simulations validating accuracy, convergence, and computational efficiency; (iv) a discussion of ill-posedness, temporal error saturation, and possible improvements using higher-order fractional order finite difference schemes and adaptive time-stepping.

2. Exact solution of the inverse problem

In this section, we shall investigate Eq (1.1). Let $\{\rho_n(x,y)\}_{n=1}^{\infty}$ be the eigenfunctions of Eq (1.2):

$$-\Delta\rho_n = \lambda_n\rho_n, \quad \rho_n|_{\partial\Omega} = 0, \quad \lambda_j > 0. \tag{2.1}$$

The unknown functions are given as follows:

$$w(x,y,t) = \sum_{j=1}^{\infty} W_j(t)\rho_j(x,y), \tag{2.2}$$

$$S(x,y) = \sum_{j=1}^{\infty} S_j\rho_j(x,y), \tag{2.3}$$

$$f(x,y,t) = \sum_{j=1}^{\infty} F_j(t)\rho_j(x,y). \tag{2.4}$$

Substituting into Eq (1.1) yields, for each mode j,

$${}_0^C D_t^{\alpha} W_j(t) = -\lambda_j W_j(t) + v(t)S_j + F_j(t). \tag{2.5}$$

From formula (2.4), we obtain

$${}_0^C D_t^{\alpha} W_j(t) + \lambda_j W_j(t) = K_j(t), \tag{2.6}$$

where

$$K_j(t) = v(t)S_j + F_j(t).$$

From Eq (2.6), we can find

$$W_j(t) = W_j(0)\,E_{\alpha}(-\lambda_j t^{\alpha}) + \int_0^t (t-z)^{\alpha-1}E_{\alpha,\alpha}(-\lambda_j(t-z)^{\alpha})K_j(z)\,dz. \tag{2.7}$$

Here, $E_\alpha(\cdot)$ and $E_{\alpha,\alpha}(\cdot)$ demonstrate the one and two parameter Mittag–Leffler functions. Therefore, we can find the exact solution of the IP as follows:

$$w(x,y,t) = \sum_{j=1}^{\infty} \left[W_j(0) E_\alpha(-\lambda_j t^\alpha) + \int_0^t (t-z)^{\alpha-1} E_{\alpha,\alpha}(-\lambda_j (t-z)^\alpha)\big(v(z) S_j + F_j(z)\big)\, ds \right] \rho_j(x,y). \quad (2.8)$$

From Eq (2.5), we have

$$v(t) S_j = {}_0^C D_t^\alpha W_j(t) + \lambda_j W_j(t) - F_j(t). \quad (2.9)$$

Hence, finally, we can obtain

$$S_j = \frac{{}_0^C D_t^\alpha W_j(t) + \lambda_j W_j(t) - F_j(t)}{v(t)}. \quad (2.10)$$

This equation provides the right-hand side independently of t. Finally,

$$S(x,y) = \sum_{j=1}^{\infty} S_j \rho_j(x,y). \quad (2.11)$$

The following separability condition has to hold for the existence of a time-independent inverse term $S(x,y)$:

$${}_0^C D_t^\alpha w(x,y,t) - \Delta w(x,y,t) - f(x,y,t) = v(t)\, q(x,y), \quad (2.12)$$

in which case

$$S(x,y) = q(x,y). \quad (2.13)$$

3. Finite difference method

Let for $k = 0, 1, \ldots, N$, $t_k = k\tau$, and $\tau = T/N$. FOCD at time t_{k+1} is approximated by applying the L1 scheme [19]:

$${}_0^C D_t^\alpha w_j^{k+1} \approx \frac{1}{\tau^\alpha} \sum_{j=0}^{k} r_j \left(w_j^{k+1-j} - w_j^{k-j} \right), \quad (3.1)$$

with coefficients

$$r_j = (j+1)^{1-\alpha} - j^{1-\alpha}, \quad j \geq 0.$$

Suppose that $h = 1/M$ is the space step size. The Laplacian operator is approximated by the standard second-order central FDS [20]:

$$\Delta_h w_n^k = \frac{w_{n+1,i}^k - 2w_{n,i}^k + w_{n-1,i}^k}{h^2} + \frac{w_{n,i+1}^k - 2w_{n,i}^k + w_{n,i-1}^k}{h^2}. \quad (3.2)$$

The BVP is applied directly by setting the numerical solution to zero at the boundary grid points. Using formulas (3.1) and (3.2), we can obtain

$$\frac{1}{\tau^\alpha} \sum_{j=0}^{k} r_m (w_n^{k+1-j} - w_n^{k-j}) = \frac{1}{2}\left(\Delta_h w_n^{k+1} + \Delta_h w_n^k \right) + v_k S_n^k, \quad 0 < \alpha \leq 1. \quad (3.3)$$

Here,

$$v_k = \frac{1}{2}\left(v^{k+1} + v^k \right) + f_{n,i}^k.$$

From the fully discrete scheme (3.3), the unknown source term S_n can be obtained as

$$S_n^k = \frac{\frac{1}{\tau^\alpha}\sum_{j=0}^{k} r_j(w_n^{k+1-j} - w_n^{k-j}) - \frac{1}{2}(\Delta_h w_n^{k+1} + \Delta_h w_n^k)}{v_k}. \tag{3.4}$$

Collecting the discrete equations for all spatial nodes and time levels yields a linear system:

$$\mathcal{K}S = W_T - w_{\text{hom}}, \tag{3.5}$$

where S is the vector form of S_n, and W_T denotes the final-time measurement data. The unknown function S_n is treated as an additional discrete variable and reconstructed by solving this algebraic system using Tikhonov regularization.

3.1. Stability estimates and convergence

In this subsection, we shall consider stability estimates and convergence for the IP used by CN-FDS. The unified effects of nonlocality and stability provide the numerical treatment of FOTDPDE, which is highly nontrivial. The presented CN-FDS successfully handles these challenges, providing stable and accurate reconstructions validated by numerical examples. We can present the following for the stability inequality theorem of formula (3.3).

Theorem 3.1. *The FDS* (3.3) *for the IBVP* (1.1)–(1.3) *is unconditionally stable in the discrete* L^2 *norm.*

Proof. We can define the inner product in the discrete L^2 norm as

$$\langle u, v\rangle = h^2 \sum_{i,j} u_{i,j} v_{i,j}, \qquad \|u\|^2 = \langle u, u\rangle,$$

where the summation process is performed across all internal grid points. Using [21] and taking the fully discrete scheme for the inner product (3.3) with w^{n+1} yields

$$\left\langle \frac{1}{\tau^\alpha}\sum_{j=0}^{k} r_j\left(w_n^{k+1-j} - w_n^{k-j}\right), w_n^{k+1}\right\rangle = \left\langle \frac{1}{2}\Delta_h w_n^{k+1} + \frac{1}{2}\Delta_h w_n^k + pS_n\right\rangle, \tag{3.6}$$

where $S_{n,i} = S_n$. First, we investigate the temporal fractional order term. Using the positivity and monotonicity of the L1 coefficients $r_j > 0$, together with the following equality,

$$\langle y - z, y\rangle = \frac{1}{2}\left(\|y\|^2 - \|z\|^2 + \|y - z\|^2\right).$$

It follows that

$$\left\langle \sum_{j=0}^{k} r_j(w_n^{k+1-j} - w_n^{k-j}), w_n^{k+1}\right\rangle \geq \frac{r_0}{2}\left(\|w_n^{k+1}\|^2 - \|w_n^k\|^2\right).$$

Second, we are dealing with spatial terms. By using the discrete Green's formula and applying the homogeneous DBCs, we get

$$\langle \Delta_h w_n^{k+1}, w_n^{k+1}\rangle = -\|\nabla_h w_n^{k+1}\|^2,$$

and

$$\langle \Delta_h w_n^k, w_n^{k+1} \rangle \leq \frac{1}{2}\|\nabla_h w_n^k\|^2 + \frac{1}{2}\|\nabla_h w_n^{k+1}\|^2.$$

For this source term, Young's inequality presents

$$\left\langle vS_n, w_n^{k+1} \right\rangle \leq \varepsilon \|w_n^{k+1}\|^2 + C_\varepsilon (|v|)^2 \|S_n\|^2,$$

for any $\varepsilon > 0$. Choosing ε a sufficiently small and substituting the above estimates into (3.6), we have

$$\|w_n^{k+1}\|^2 - \|w_n^k\|^2 + \tau^\alpha \|\nabla_h w_n^{k+1}\|^2 \leq C\tau^\alpha (|v|)^2 \|S_n\|^2.$$

Using the discrete Poincaré inequality,

$$\|w_n^{k+1}\|^2 \leq C\|\nabla_h w_n^{k+1}\|^2,$$

and attracting the gradient term, we get

$$\|w_n^{k+1}\|^2 \leq \|w_n^k\|^2 + C\Delta t^\alpha \|S_n\|^2.$$

Taking the square root of the last formula, we arrive at

$$\|w_n^{k+1}\| \leq \|w_n^k\| + C\|S_n\|.$$

Finally, by induction on k, we can obtain

$$\|w_n^k\| \leq \|w_n^0\| + CT\|S_n\|, \quad k = 1, 2, \ldots, N.$$

In conclusion, this shows that the numerical solution is obtained, bounded independently of τ and h. Therefore, the CN-FDS is unconditionally stable. □

3.2. Convergence analysis

Now, we establish the convergence of the proposed CN-FDS for the FOTDPDE. Let $w(x, y, t)$ be the analytical solution of the continuous problem and $w_{n,i}^k$ denote the numerical approximation at the grid point (x_n, y_i, t_k). Define the global error function as

$$e_{n,i}^k = w(x_n, y_i, t_k) - w_{n,i}^k.$$

3.3. Local truncation error

Suppose that the analytical solution $w(x, y, t)$ is sufficiently smooth. By using Taylor expansions in time and space and using the L1 approximation for the FOCD, the local truncation error $R_{i,n}^{k+1}$ satisfies

$$\|R^{k+1}\| \leq C\left(\tau^{2-\alpha} + h^2\right), \tag{3.7}$$

where $h = \max(h_x, h_y)$ and $C > 0$ is a constant and that does not depend on τ and h. Now, we shall present the convergence theorem as follows:

Theorem 3.2. *Asuume that $0 < \alpha \leq 1$, and let the analytical solution $w(x, y, t) \in C^2([0, T]; H^2(\Omega))$. Then, CN-FDS for the inverse problem of time-FOTDPDE is convergent, and the approximate solution satisfies the error estimate*

$$\|e^k\| \leq C\left(\tau^{2-\alpha} + h^2\right), \quad 1 \leq k \leq N,$$

where C is a constant and not dependent on τ, h, and k.

Proof. Subtracting the numerical FDS from the continuous equation evaluated at the grid points gives the discrete error equation

$$ {}_0^C D_t^{\alpha} e^{k+1} - \Delta_h e^{k+\frac{1}{2}} = R^{k+1}, \tag{3.8}$$

where Δ_h denotes the standard five-point discrete Laplacian. Using the discrete inner product of (3.8) with e^{k+1} and summing over all interior grid points, we get

$$\left\langle {}_0^C D_t^{\alpha} e^{k+1}, e^{k+1} \right\rangle + \frac{1}{2}\|\nabla_h e^{k+1}\|^2 \leq \frac{1}{2}\|\nabla_h e^k\|^2 + \langle R^{k+1}, e^{k+1}\rangle.$$

Applying the positivity of the L1 coefficients and using Young's inequality, the right-hand side can be bounded as

$$\langle R^{k+1}, e^{k+1}\rangle \leq \frac{1}{2}\|e^{k+1}\|^2 + C\|R^{k+1}\|^2.$$

By the truncation error estimate and the discrete Poincaré inequality (3.7), it follows that

$$\|e^{k+1}\| \leq \|e^k\| + C\left(\tau^{2-\alpha} + h^2\right).$$

Using this mathematical induction over k, the proof of this theorem is completed and has established the stated convergence rate. □

Definition 3.1 (Experimental order of convergence)**.** Let w be the analytical solution of the continuous problem, and let w_h denote the corresponding approximate solution obtained on a spatial mesh with mesh size h. Denote by $E(h)$ the numerical error measured in a suitable norm, that is,

$$E(h) = \|w(\cdot, T) - w_h^N\|,$$

where w_h^N denotes the fully discrete numerical solution at the final time T. Given two successive mesh sizes k_1 and k_2 with $k_2 < k_1$, the *experimental order of convergence* (EOC) is defined by

$$\text{EOC} = \frac{\log(E(k_1)/E(k_2))}{\log(k_1/k_2)}.$$

Using Matlab programming for EOC and the maximum error, we can obtain Tables 1 and 2 as follows:

Table 1. Maximum error and EOC for $\alpha = 0.25$ at $T = 1$.

$N_x = N_y$	Maximum error	EOC
10	2.217×10^{-3}	–
20	5.868×10^{-4}	1.918
40	1.393×10^{-4}	2.075
80	2.794×10^{-5}	2.3185

Table 2. Maximum error and EOC for $\alpha = 0.75$ at $T = 1$.

$N_x = N_y$	Maximum error	EOC
10	2.381×10^{-3}	–
20	6.716×10^{-4}	1.826
40	1.824×10^{-4}	1.880
80	4.970×10^{-5}	1.876

From Tables 1 and 2, a rapid reduction of the error is observed when the mesh is refined from $N_x = 10$ to $N_x = 80$, obtaining a large EOC value. This behavior demonstrates that, beyond a certain spatial resolution, the numerical error is no longer dominated by spatial decomposition. Instead, the error reaches saturation due to the temporal decomposition of the FOCD and the accumulation of past terms in the L1 approximation. Consequently, simply improving the spatial grid does not increase overall accuracy. These results confirm that the proposed scheme is stable and converges, while also highlighting the need for a balanced improvement strategy in both space and time when solving fractional inverse problems. Similar saturation events have been reported in the literature for time-FTDPDE. Although the definitions presented in this section are classical, they are essential for the formulation of the proposed CN-FDS; the stability estimates and convergence analysis for the analysis of the two-dimensional inverse problem developed in this section are presented for the first time, specifically for this problem. To investigate the robustness of the proposed inverse algorithm, we consider a noisy measurement scenario. The final-time data are perturbed by additive Gaussian noise, i.e.,

$$w^{\delta}(x, y, T) = w(x, y, T) + \delta \cdot \mathcal{N}(0, 1),$$

where δ shows the noise level and $\mathcal{N}(0, 1)$ is a standard normal random variable. We test the algorithm for noise levels $\delta = 1\%, 3\%, 5\%$ in Table 3. The reconstructed source term remains stable and accurate, demonstrating the robustness of the proposed numerical scheme against data perturbations.

Table 3. Influence of Gaussian noise on the numerical reconstruction.

Noise level δ	Max absolute error	Relative error
0	6.715929×10^{-4}	1.835831×10^{-3}
0.01	7.171787×10^{-4}	1.960442×10^{-3}
0.03	9.710220×10^{-4}	2.654335×10^{-3}
0.05	1.027971×10^{-3}	2.810006×10^{-3}

Figure 1 shows the influence of Gaussian noise on the numerical reconstruction with various δ and $\alpha = 0.75$.

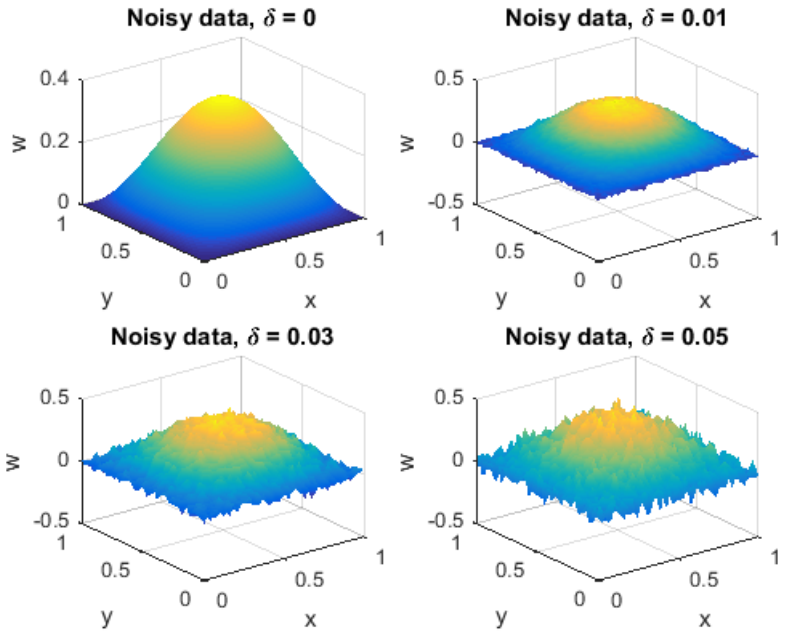

Figure 1. Influence of Gaussian noise on the numerical reconstruction with various δ and $\alpha = 0.75$.

4. Results

In this section, an approximate example is presented to validate the proposed CN-FDS for the fractional time-dependent PDE. Numerical experiments are carried out to verify the stability and accuracy of the given method. A manufactured exact solution satisfying the IBVP is employed to evaluate the numerical error. The maximum error at the final time T is given by

$$\text{Max Error} = \max_{n,i} \left| w_{n,i}^{\text{numerical}} - w_{n,i}^{\text{exact}} \right|,$$

and

$$\text{Relative Error} = \frac{\max\limits_{n,i} \left| w_{n,i}^{\text{numerical}} - w_{n,i}^{\text{exact}} \right|}{\max\limits_{n,i} \left| w_{n,i}^{\text{exact}} \right|}.$$

4.1. Numerical results

Consider the following numerical example of a fractional time-dependent PDE (FTDPDE) with IBV and inverse conditions:

$$\begin{cases} {}_0^C D_t^\alpha w(x,y,t) = \Delta w(x,y,t) + v(t)S(x,y) + f(x,y,t), & (x,y) \in \Omega,\ 0 < t \le 1, \\ w(x,y,0) = 0, & (x,y) \in \Omega, \\ w(x,y,t) = 0, & (x,y) \in \partial\Omega,\ 0 < t \le 1, \\ w\left(x,y,\frac{1}{2}\right) = e^{-\frac{1}{2}}\left(\frac{1}{2}\right)^2 \sin(\pi x)\sin(\pi y), & (x,y) \in \Omega, \end{cases} \tag{4.1}$$

where $0 < \alpha \le 1$, and $\Omega = (0,1) \times (0,1)$. The memory term is presented by

$$v(t)S(x,y) = t^2 \sin(\pi x)\sin(\pi y),$$

and the source term $f(x,y,t)$ is chosen such that the exact solution is

$$w_{\text{exact}}(x,y,t) = e^{-t}t^2 \sin(\pi x)\sin(\pi y), \tag{4.2}$$

and

$$\begin{aligned} f(x,y,t) &= {}_0^C D_t^\alpha u_{\text{exact}}(x,y,t) - \Delta u_{\text{exact}}(x,y,t) - h(t)p(x,y) \\ &= \sin(\pi x)\sin(\pi y)\left(\sum_{k=0}^{\infty} \frac{(-1)^k \Gamma(k+3)}{k!\,\Gamma(k+3-\alpha)} t^{k+2-\alpha} + 2\pi^2 e^{-t}t^2 - t^2\right). \end{aligned}$$

As a CN finite difference scheme corresponding to eq (4.1),

$$\begin{aligned} &\frac{1}{\Gamma(2-\alpha)\Delta t^\alpha}\left(w_{n,i}^{k+1} - \sum_{j=1}^{k-1} r_j \left(w_{n,i}^{k+1-j} - w_{n,i}^{k-j}\right)\right) \\ &= \frac{1}{2}\left[\frac{w_{n+1,i}^{k+1} - 2w_{n,i}^{k+1} + w_{n-1,i}^{k+1}}{\Delta x^2} + \frac{w_{n,i+1}^{k+1} - 2w_{n,i}^{k+1} + w_{n,i-1}^{k+1}}{\Delta y^2}\right. \\ &\left. + \frac{w_{n+1,i}^{k} - 2w_{n,i}^{k} + w_{n-1,i}^{k}}{\Delta x^2} + \frac{w_{n,i+1}^{k} - 2w_{n,i}^{k} + w_{n,i-1}^{k}}{\Delta y^2}\right] + v(t_{n+1/2})S_{n,i} + f_{n,i}^{k+1/2}, \end{aligned} \tag{4.3}$$

can be written, where $r_j = (j+1)^{1-\alpha} - j^{1-\alpha}$, and the indices $n = 1, \ldots, N_x$, $i = 1, \ldots, N_y$ correspond to the spatial grid. The initial and boundary values are imposed as

$$w_{n,i}^0 = 0, \quad w_{0,i}^k = w_{N_x+1,i}^k = w_{n,0}^k = w_{n,N_y+1}^k = 0,$$

with the inverse term applied at the discrete mid-step:

$$w_{n,i}^{k_m} = e^{-t_{k_m}} t_{k_m}^2 \sin(\pi x_i)\sin(\pi y_j), \quad t_{k_m} = \frac{T}{2}.$$

Now, we will compare the analytical and numerical solutions. For the approximate solution of eq (1.1), CN-FDS is used, given in the formula (3.3). Here, uniform spatial grids $\Delta x = \Delta y = h$ and a uniform time step τ are employed. Figure 2 represents the convergence behavior of the numerical finite scheme method at $y = 0$, with $\alpha = 0.5$. Figure 3 reveals an error saturation phenomenon for sufficiently fine spatial discretizations. This behavior is not caused by numerical instability, but rather by the intrinsic memory effect of the fractional operator and the ill-posed nature of the inverse boundary

value problem. Similar saturation effects have been reported in fractional diffusion and inverse heat conduction problems. A graded temporal mesh $t_k = (k/N)^r T$, with $r > 1/\alpha$, can be used to improve convergence, which is a promising direction for future research.

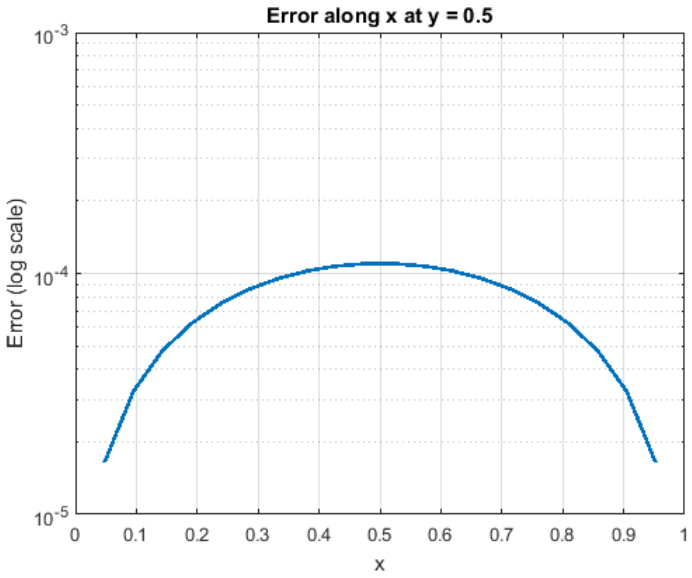

Figure 2. Error (log scale) calculated for along x at $y = 0$, and $\alpha = 0.5$.

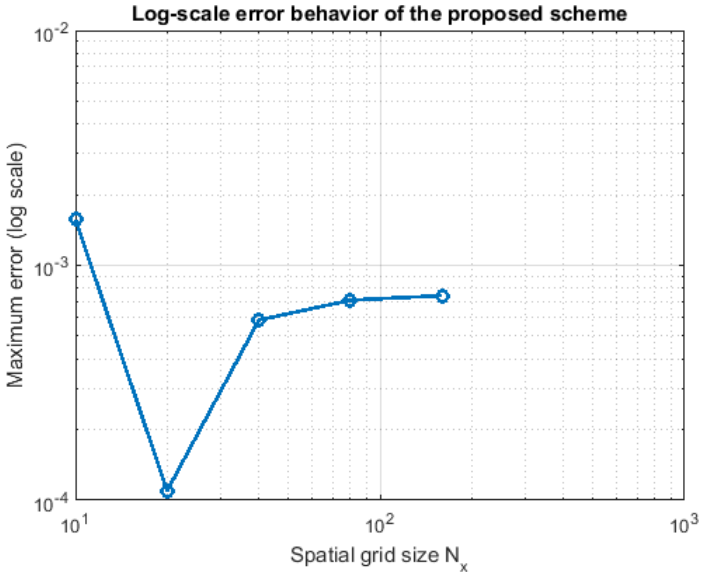

Figure 3. Maximum error (log scale) calculated for $Nx = N_y \in \{10, 20, 40, 80, 160\}$, $T = 1$, and $\alpha = 0.5$.

Figure 4 shows smooth and bounded behavior throughout the computational domain, with maximum values concentrated near the boundary. This figure supports the stability and convergence of the finite difference method. Although similar figure representations are commonly used, the presented

figures show the behavior of the proposed CN-FDS for a FOTDPDE, which has not been previously investigated. Figure 5 calculates the exact solution for Eq (4.1). Figure 6 gives an approximate solution for Eq (3.3) by using FDM.

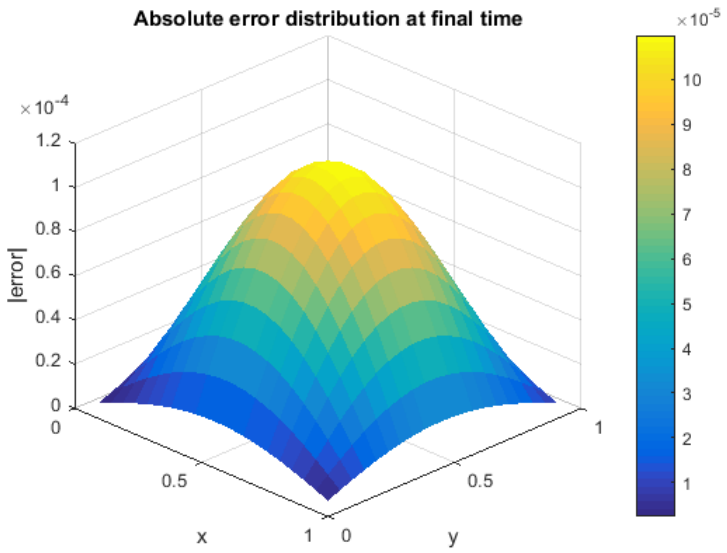

Figure 4. Absolute error distribution calculated along x and y, $T = 1$, and $\alpha = 0.5$.

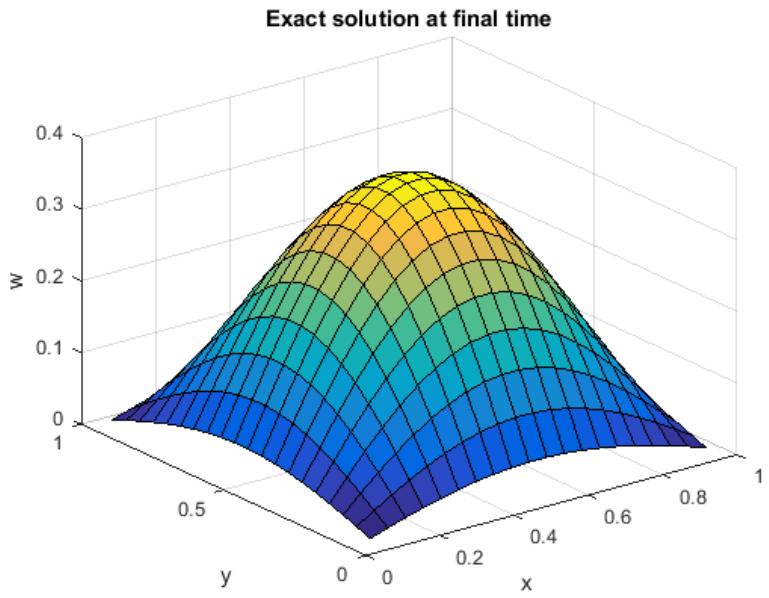

Figure 5. Exact solution calculated along x and y, $T = 1$, and $N_x = N_y = 80$.

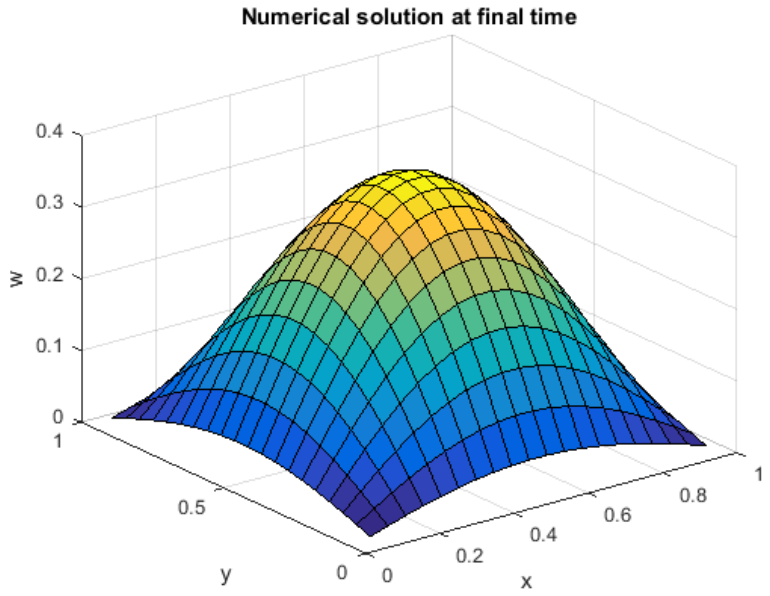

Figure 6. Numerical solutions calculated along x and y, $T = 1$, $\alpha = 0.5$, and $N_x = N_y = 40$.

Figure 7 shows smooth and bounded behavior, confirms the stability of the approximate finite difference scheme, and highlights the memory effect induced by the fractional time derivative. Figure 8 compares the exact solution (4.2) and approximate solution (3.3). From this figure, the CN-FDS method is an effective method for this model because the two methods have very close results.

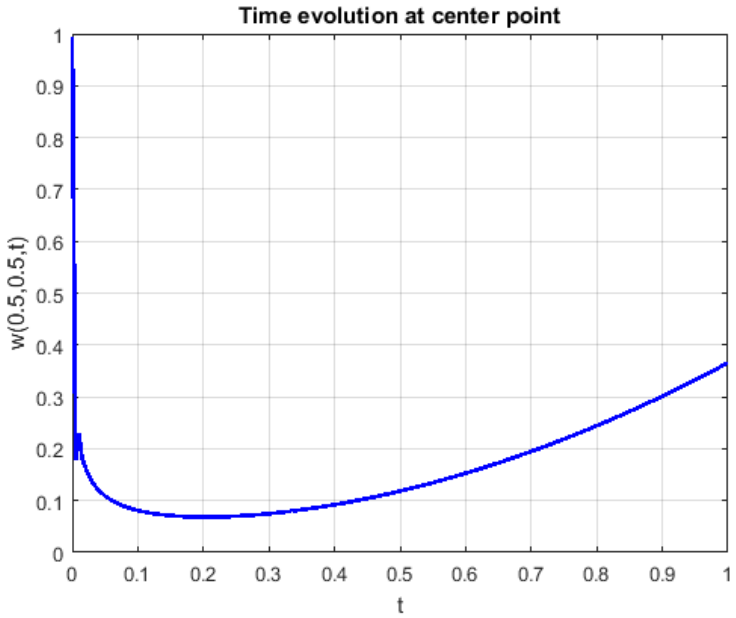

Figure 7. Time evolution at center point for $\alpha = 0.5$ and $N_x = N_y = 40$.

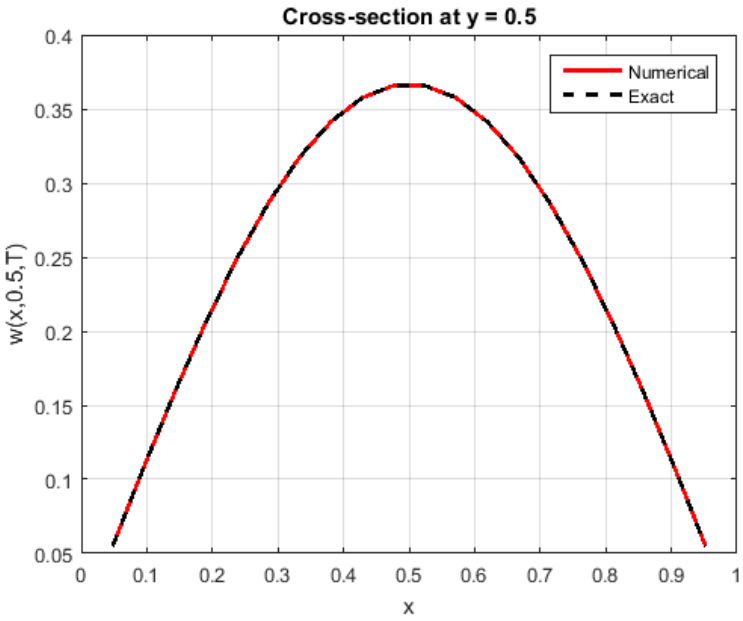

Figure 8. Comparison exact and numerical solutions for $\alpha = 0.5$, $x = y = 0.5$, $T = 1$, and $N_x = N_y = 40$.

Figure 9 shows the error $|w_{\text{exact}}(x, y, 1) - w_{\text{num}}(x, y, 1)|$ and the spatial–temporal distribution of numerical errors. Figure 10 exhibits a uniform and stable spatial distribution consistent with the applied boundary conditions.

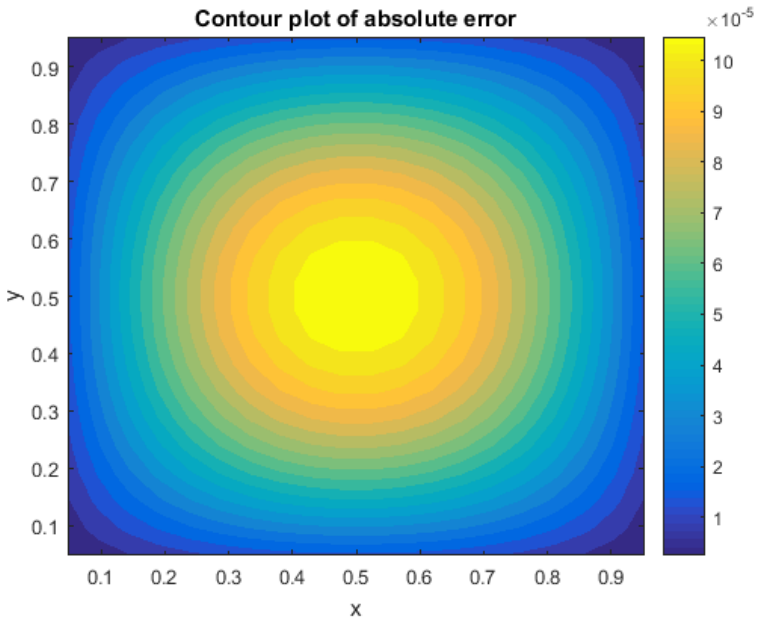

Figure 9. Contour plot of absolute error calculated for the exact and approximate solution at x and y, $T = 1$, and $\alpha = 0.5$.

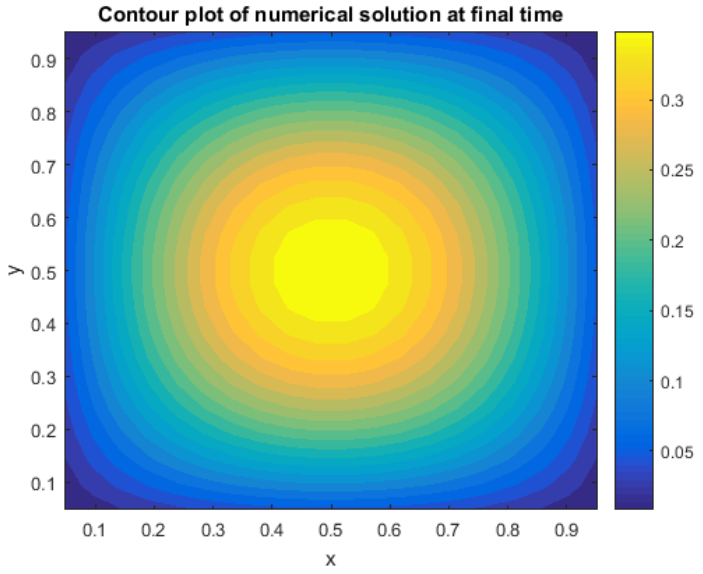

Figure 10. Contour plot of the numerical solution at final time for $\alpha = 0.5$, $(x, y) \in [0, 1] \times [0, 1]$, $T = 1$, and $N_x = N_y = 40$.

Figure 11 demonstrates that the source term has been recovered consistently and accurately. Figure 12 shows the effect of fractional order α and compares different α values. From Table 4, fractional order α values give very good results from integer order derivatives.

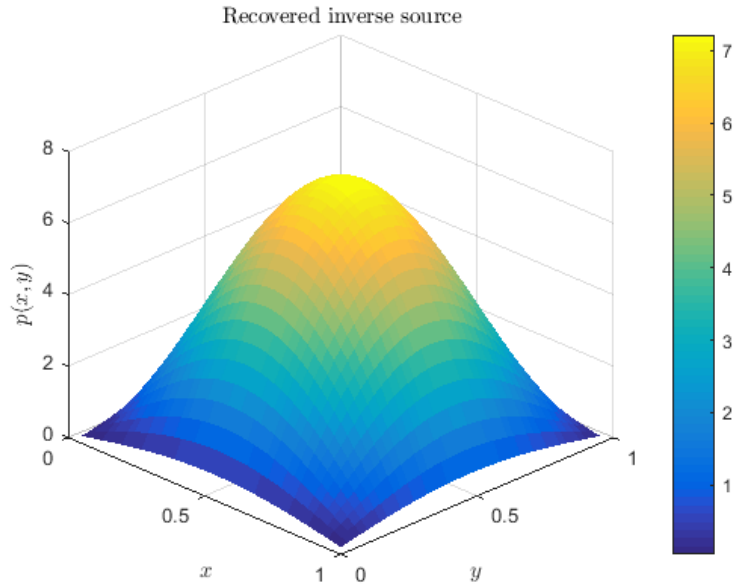

Figure 11. Inverse source figure for $N_x = N_y = 40$, $N_t = 200$, and $\alpha = 0.5$.

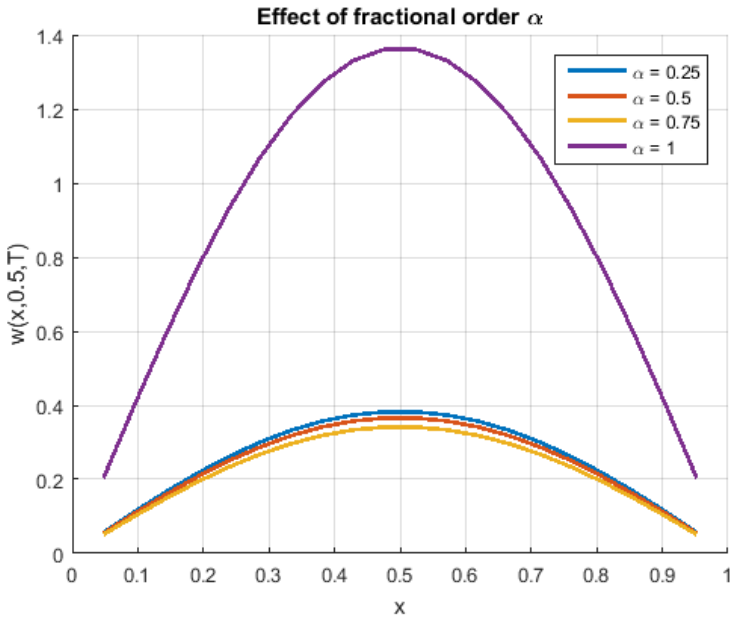

Figure 12. Calculations for values in the following table.

Table 4. Maximum error and relative error for different α.

α	$N_x = N_y = 5N_t$	Max error	Relative error
0.25	10	4.139169×10^{-3}	7.804201×10^{-3}
	20	1.206283×10^{-3}	2.240838×10^{-3}
	40	3.542937×10^{-4}	6.554355×10^{-4}
0.50	10	4.420597×10^{-3}	8.334820×10^{-3}
	20	1.346492×10^{-3}	2.501295×10^{-3}
	40	4.210945×10^{-4}	7.790155×10^{-4}
0.75	10	4.632520×10^{-3}	8.734390×10^{-3}
	20	1.437982×10^{-3}	2.671250×10^{-3}
	40	4.626832×10^{-4}	8.559537×10^{-4}
1.00	10	3.251914×10^{-3}	6.131325×10^{-3}
	20	3.666938×10^{-4}	6.811844×10^{-4}
	40	4.422349×10^{-4}	8.181248×10^{-4}

Remark 4.1. *For fractional orders* $0 < \alpha < 1$*, the Caputo derivative operator introduces a memory effect in time:*

$$ {}_0^C D_t^\alpha w(t) = \frac{1}{\Gamma(1-\alpha)} \int_0^t \frac{w'(\tau)}{(t-\tau)^\alpha} d\tau. $$

This integral depends on all previous time steps, which has a smoothing effect on the solution. When discretized with the L1 formula, the approximation effectively averages contributions from the solution history, providing a numerical damping that reduces the impact of time discretization errors. As a result, the computed solution for $\alpha < 1$ often exhibits smaller maximum and relative errors

compared to the classical case $\alpha = 1$. In contrast, for $\alpha = 1$, the Caputo derivative reduces to the standard first-order time derivative:

$$ {}_0^C D_t^1 w = w_t, $$

and the L1 formula is no longer optimal. Here, the solution depends only on the current time step, exposing the full time discretization error and leading to larger errors unless the temporal grid is refined.

5. Discussion

Table 2 presents the EOC and maximum error for the proposed method. This table was used to calculate and compare maximum error margins for different ranges. Table 4 compares derivatives of different fractional orders α. From this table, it is clear that the approximate solutions obtained for fractional-order derivatives are better and more efficient than those obtained for integer-order derivatives. Various numerical approaches have been developed for time-fractional diffusion inverse problems, including spectral methods and finite element methods (FEM). Spectral methods provide very high accuracy for smooth solutions but require global basis functions and are less flexible for complex geometries. FEM is well-suited for irregular domains but involves a higher computational cost and more complex implementation. In contrast, the proposed Crank–Nicolson finite difference scheme (CN-FDS) is simple to implement, computationally efficient, and well-suited for structured grids. Moreover, CN-FDS leads to sparse linear systems and is easily extendable to higher dimensions. These features make the proposed method attractive for practical inverse problems.

6. Conclusions

A stable finite difference method has been constructed for the inverse problem of the two-dimensional time-dependent fractional diffusion boundary value problem. The proposed approach combines the L1 approximation for the Caputo fractional derivative with the Crank–Nicolson scheme for space decomposition. A rigorous stability analysis proves the unconditional stability of the method. Numerical experiments confirm the efficiency and reliability of the scheme. Numerical experiments demonstrate that the proposed method accurately reconstructs the solution to the inverse source problem. The agreement between the numerical and exact solutions confirms the effectiveness of the CN-FDM decomposition combined with the L1 approximation for the Caputo fractional order derivative. This study is limited to structured grids and synthetic test problems. Higher-order fractional order finite difference schemes, adaptive time decomposition, and extensions to real noisy data will be investigated in future research.

Author contributions

The authors contributed equally to this work. All authors read and approved the final manuscript.

Use of Generative-AI tools declaration

The authors declare that they have not used Artificial Intelligence (AI) tools in the creation of this article.

Funding

The authors received no financial support for the research, authorship, and/or publication of this article.

Acknowledgments

The authors are very grateful to anonymous referees for their careful reading and valuable comments which led to the improvement of this manuscript.

Conflict of interest

The authors declare no conflicts of interest.

References

1. S. N. Antontsev, S. E. Aitzhanov, G. R. Ashurova, An inverse problem for the pseudo-parabolic equation with p-Laplacian, *Evol. Equ. Control The.*, **11** (2022), 399–414. http://doi.org/10.3934/eect.2021005
2. K. Khompysh, M. Ruzhansky, Inverse source problems for time-fractional nonlinear pseudoparabolic equations with p-Laplacian, *Fract. Calc. Appl. Anal.*, **28** (2025), 1353–1383. https://doi.org/10.1007/s13540-025-00404-6
3. F. Huang, F. Liu, The time fractional diffusion equation and the advection-dispersion equation, *ANZIAM J.*, **46** (2005), 317–330. hhttps://doi.org/10.1017/S1446181100008282
4. N. H. Sweilam, H. Moharram, N. K. A. Moniem, S. Ahmed, A parallel Crank–Nicolson finite difference method for time-fractional parabolic equation, *J. Numer. Math.*, **22** (2014), 363–382. https://doi.org/10.1515/jnma-2014-0016
5. A. Akgül, M. Modanli, Crank–Nicholson difference method and reproducing kernel function for third order fractional differential equations in the sense of Atangana–Baleanu Caputo derivative, *Chaos Soliton. Fract.*, **127** (2019), 10–16. https://doi.org/10.1016/j.chaos.2019.06.011
6. M. Modanli, K. Karadag, S. T. Abdulazeez, Solutions of the mobile-immobile advection-dispersion model based on the fractional operators using the Crank–Nicholson difference scheme, *Chaos Soliton. Fract.*, **167** (2023), 113114. https://doi.org/10.1016/j.chaos.2023.113114
7. K. Oishi, Y. Hashizume, T. Nakao, K. Kashima, Extraction of implicit field cost via inverse optimal Schrödinger bridge, *SICE Journal of Control, Measurement, and System Integration*, **18** (2025), 2490332. https://doi.org/10.1080/18824889.2025.2490332
8. S. E. Chorfi, A. Hasanov, R. Morales, Identification of source terms in the Schrödinger equation with dynamic boundary conditions from final data, *Z. Angew. Math. Phys.*, **76** (2025), 127. https://doi.org/10.1007/s00033-025-02505-x
9. E. Shivanian, A. Jafarabadi, M. J. Huntul, A local meshless technique for recovering dual forms of time-varying sources in the nonlocal inverse heat equation, *Results in Applied Mathematics*, **28** (2025), 100673. https://doi.org/10.1016/j.rinam.2025.100673

10. S. S. Liu, L. X. Feng, An inverse problem for a two-dimensional time-fractional sideways heat equation, *Math. Probl. Eng.*, **2020** (2020), 5865971. https://doi.org/10.1155/2020/5865971
11. T. Liu, F. Soleymani, M. Z. Ullah, Solving multi-dimensional European option pricing problems by integrals of the inverse quadratic radial basis function on non-uniform meshes *Chaos Soliton. Fract.*, **185** (2024), 115156. https://doi.org/10.1016/j.chaos.2024.115156
12. T. Liu, Parameter estimation with the multigrid-homotopy method for a nonlinear diffusion equation, *J. Comput. Appl. Math.*, **413** (2022), 114393. https://doi.org/10.1016/j.cam.2022.114393
13. W. Hu, Z. J. Fu, Z. C. Tang, Y. Gu, A meshless collocation method for solving the inverse Cauchy problem associated with the variable-order fractional heat conduction model under functionally graded materials, *Eng. Anal. Bound. Elem.*, **140** (2022), 132–144. https://doi.org/10.1016/j.enganabound.2022.04.007
14. Z. J. Fu, L. W. Yang, Q. Xi, C. S. Liu, A boundary collocation method for anomalous heat conduction analysis in functionally graded materials *Comput. Math. Appl.*, **88** (2021), 91–109. https://doi.org/10.1016/j.camwa.2020.02.023
15. L. D. Long, B. P. Moghaddam, Y. Gurefe, Iterative weighted Tikhonov regularization technique for inverse problems in time-fractional diffusion-wave equations within cylindrical domains, *Comp. Appl. Math.*, **44** (2025), 215. https://doi.org/10.1007/s40314-025-03176-0
16. R. Brociek, A. Wajda, C. Napoli, G. Capizzi, D. Słota, An inverse problem for a fractional space-time diffusion equation with fractional boundary condition, *Entropy*, **28** (2026), 81. https://doi.org/10.3390/e28010081
17. H. M. Zhu, J. Zheng, Z. Y. Zhang, Approximate symmetry of time-fractional partial differential equations with a small parameter, *Commun. Nonlinear Sci.*, **125** (2023), 107404. https://doi.org/10.1016/j.cnsns.2023.107404
18. I. Podlubny, *Fractional differential equations: An introduction to fractional derivatives, fractional differential equations, to methods of their solution and some of their applications*, San Diego: Academic Press, 1998.
19. S. T. Abdulazeez, M. Modanli, Solutions of fractional order pseudo-hyperbolic telegraph partial differential equations using finite difference method, *Alex. Eng. J.*, **61** (2022), 12443–12451. https://doi.org/10.1016/j.aej.2022.06.027
20. M. Nitiema, T. Tindano, W. Some, Crank–Nicolson method for the advection-diffusion equation involving a fractional Laplace operator, *Abstr. Appl. Anal.*, **2025** (2025), 6642234. https://doi.org/10.1155/aaa/6642234
21. M. Abdalla, F. Bourse, A. De Caro, D. Pointcheval, Simple functional encryption schemes for inner products, In: *Public-Key Cryptography–PKC 2015*, Berlin: Springer, 2015, 733–751. https://doi.org/10.1007/978-3-662-46447-2_33